Nonresonant absorption of pulsed ruby laser radiation by atmospheric air and H_2O–nitrogen mixture

B.A. Tikhomirov, A.B. Tikhomirov, and K.M. Firsov

Institute of Atmospheric Optics,
Siberian Branch of the Russian Academy of Sciences, Tomsk

Received April 16, 2001

Coefficients of weak nonresonant absorption of pulsed ruby laser radiation (λ = 694.300 nm) by binary mixtures of water vapor with atmospheric air and nitrogen were measured for the first time using time resolved photo-acoustic technique with the threshold sensitivity $k_\lambda^{\min} \le 10^{-8}$ cm^{-1}. The results of our study confirm the earlier conclusion of other authors that there is some substance in the atmosphere responsible for excess absorption of short-ware radiation.

Introduction

Possible physical effects determining the nature of excess absorption of the shortwave (0.44 – 3.97 μm) optical radiation in clouds[2,3] and on long paths under natural conditions[4–6] were discussed in the paper by Pkhalagov et al.[1] The term "excess absorption" is used in the literature to mean a discrepancy between the experimental data and model calculations. It was noted that understanding of the nature of the excess (anomalous) absorption observed in the experiments[2–6] is very important for quantitative estimates of main factors determining the Earth's radiative budget both in the cloudy and cloudless atmosphere.

Various possible reasons for excessive absorption of shortwave optical radiation in the atmosphere include, in particular, the water vapor continuum absorption.[1] The data of laboratory experiments, in which the information on the continuum absorption coefficient could be obtained under conditions free of interfering factors (aerosol and Rayleigh scattering, instrumental effects, etc.), are absent in the literature. In this connection, the experiments measuring the coefficient of nonresonant absorption of radiation in the shortwave spectral region by atmospheric air and its major gaseous constituents under controlled laboratory conditions is of great interest.

In this paper we report the measurement of the pulsed ruby laser radiation absorption coefficient at the wavelength of 694.300 nm by the mixtures of water vapor with nitrogen and atmospheric air at different concentrations of water vapor. For this purpose, we use the photo-acoustic laser spectroscopy technique. The obtained experimental data for every mixture are then compared with each other and with the calculated molecular absorption coefficients.

It should be noted that the data of experiments in the open atmosphere[4–6] differ from the calculated results on the water vapor continuum absorption[7,8] by 1–2 orders of magnitude. In the absolute units, the experimental data on the coefficients of the shortwave radiation absorption by atmospheric air exceed the calculated data by $\Delta k_\lambda \sim 10^{-7}$ cm^{-1} (Ref. 1). Consequently, to measure the coefficient of the excess absorption of shortwave radiation by atmospheric air under laboratory conditions, the spectrometer used should have the threshold sensitivity $k_\lambda^{\min} \le 10^{-8}$ cm^{-1} for the absorption coefficient. Therefore, our priority task was to improve the threshold sensitivity of a ruby laser PA spectrometer[9] up to 10^{-8} cm^{-1} and to perfect the measurement technique.

Measurement instrumentation

The *PA spectrometer* is shown schematically in Fig. 1. It includes a frequency-tunable ruby laser, a PA detector (PAD) with units of amplification and recording the PA signal shape, a vacuum station to pump down the PA detector cell and fill it with the gas under study, a calorimeter to measure the energy of laser pulses, and a system to measure the wavelength shift and the laser pulse spectrum.

The pulsed *Q*-switch ruby laser with the pulse-to-pulse tunable radiation wavelength includes an active element of 180 mm in length and 8 mm in diameter located inside a two-lamp elliptic water-cooled lighter. The length of the active rod with faces normal to the axis is equal to 120 mm. The back spherical mirror of the cavity with the reflection coefficient $\rho \approx 100\%$ has the curvature radius R = 100 cm. As the output laser mirror, we used the resonant reflector consisting of two plane-parallel plates. The reflector is housed in the radiator with water heating. The optical length of the cavity is $L = 0.98 \cdot R$ = 98 cm. According to Ref. 10, this length allowed us to obtain the narrowest emission spectrum for the laser with passive *Q*-switching of the plane-spherical cavity.

0235-6880/01/09 674-07 $02.00

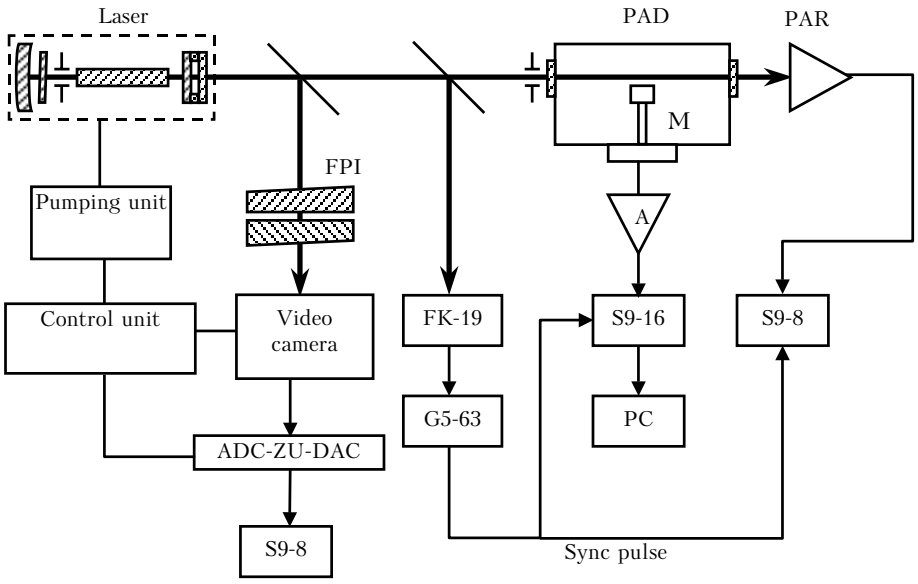

Fig. 1. PA spectrometer with ruby laser.

The pulse-to-pulse tuning of radiation wavelength λ was performed by changing the temperature of the resonant reflector t_r (continual tuning) and the temperature of the ruby rod (rough tuning). At the $\delta t_r \pm 0.02$ K accuracy of fixation of the resonant reflector temperature, the scatter in the wavelength shift from pulse to pulse did not exceed $\delta\lambda = \pm 10^{-3}$ nm. The temperature of the active element and the resonance reflector was controlled with two U4 thermostats.

For *Q*-switching and generation of giant pulses of $\tau_p \approx 50$ ns long, a passive switch made of KS-19 glass was installed right against the back mirror of the laser. For partial unloading and protection of the switch against destruction by high-power pulses, a diaphragm with a hole of about 5 mm in diameter was installed between the active element and the switch. The active element was misaligned so that the focused radiation reflected from the faces of the active element fell on the diaphragm absorbing surface.

This spectrometer, in contrast to the PA spectrometer from Ref. 9, includes the PA detector with the spatiotemporal resolution of signals. Its cylindrical absorbing cell is of 20 cm in diameter and 30 cm in length. A half-inch capacitor microphone was fixed at the center of the cell. The cell's faces were equipped with transparent windows for input and output of radiation. The separation between the laser beam and the microphone was 1.5–2 cm. Such a design of the cell allowed us to completely separate, in time, the valid PA signal caused by radiation absorption by the gas under study from parasitic background signals. The first pressure pulse acting on the microphone membrane was the pulse connected with absorption of radiation in the gas volume near the microphone, and only far later the membrane was affected by the pressure pulses caused by radiation absorption by the cell windows and walls.

The PA signal was amplified by a broadband amplifier with the gain factor $k_g = 1000$ and then came to the input of the S9-16 digital oscilloscope. The measurement error of the signal amplitude at the center of the 694.380-nm H_2O absorption line is about 1.5% according to the oscilloscope specification. The start of beam scanning in the oscilloscope was synchronized with the laser pulse with the help of the FK-19 photodetector and the G5-63 pulse generator. From the oscilloscope, the digitized PA signals came to a computer (PC) through the specialized interface.

For convenience, higher speed and accuracy of measurements of the laser pulse energy, a PA receiver (PAR) with the operation time of about 1 s was installed at the PA detector cell output. The PAR signal amplitude, proportional to the laser pulse energy, was measured by the S9-8 digital oscilloscope with the error of 1.5%. To determine the laser pulse energy in absolute units, the PAR was replaced by a serial IKT-1N calorimeter in the beginning of every measurement series. The energy of the radiation pulse was $E \approx (50 \pm 10)$ mJ.

The system for measuring the wavelength shift and spectrum of laser pulses included a Fabry–Perot interferometer, a long-focus objective, and an automatic interferogram reader based on the Elektronika L-801 video camera. The scan of the interferogram by the diameter of interference fringes was displayed on the screen of the S9-8 oscilloscope, used for measuring the pulse-to-pulse wavelength shift and the spectral width of laser pulses. In the experiment, the Fabry–Perot interferometers with the base length of 1 and 30 mm were used.

The absorption spectrum of the atmospheric air at the total pressure $P_{tot} = 1005$ mbar, temperature $T = 298$ K, and water vapor partial pressure $P_{H_2O} = 18.2$ mbar in the wavelength range of the ruby laser was calculated with the use of the HITRAN-96 databank.[11] This spectrum is depicted in Fig. 2*a*.

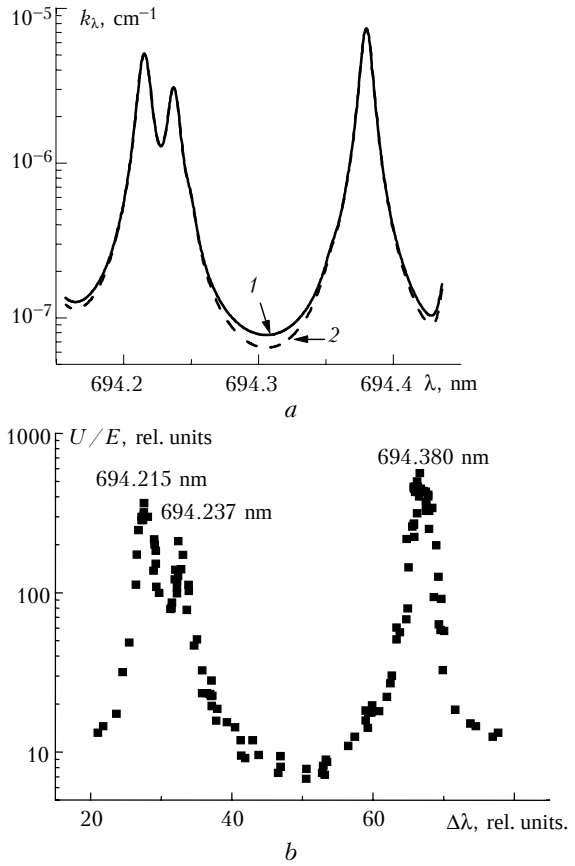

Fig. 2. Absorption spectrum of atmospheric air in the wavelength range of ruby laser (*a*). PA spectrometer signal U/E vs. the relative shift of the ruby laser wavelength. The measurements were conducted at T = 298 K, P_{tot} = 1005 mbar, and P_{H_2O} = 15.8 mbar with Fabry–Perot interferometer base length t = 1 mm (*b*).

The spectrum was calculated by the CKD0 model[12] with allowance (curve *1*) and without allowance (curve *2*) for the water vapor continuum absorption. This spectral region includes the well-known water vapor absorption lines of the $\nu_1 + 3\nu_3$ band centered at 694.215, 694.237, and 694.380 nm. Although these H_2O absorption lines were thoroughly studied experimentally,[13–16] the absorption coefficient in line wings has not been measured because of the insufficient sensitivity of spectrometers. It can be seen from Fig. 2*a* that the minimum value of the air absorption coefficient in the spectral range under consideration is $k_\lambda < 10^{-7}$ cm^{-1} at rather high humidity and even for the model accounting for the continuum absorption.

Figure 2*b* depicts the PA signal in the spectral range under consideration recorded using the PA spectrometer (see Fig. 1) with the Fabry–Perot interferometer base t = 1 mm.

The coefficients of nonresonant absorption of the 694.300 nm radiation by indoor air and the water vapor–nitrogen mixture were measured using the technique applied earlier in Refs. 17 and 18 to measurements of cross sections of the iodine laser radiation absorption by gaseous atmospheric constituents (CO_2, CH_4, H_2O). When the buffer gas pressure is much higher than the partial pressure of the absorbing gas at the fixed total pressure of the mixture, the PA spectrometer sensitivity is independent of the partial pressure of the absorbing gas,[17,18] and the amplitude of the PA spectrometer signal is proportional to the absorbing gas concentration for any radiation wavelength. Therefore, measuring the PA signal dependence on the concentration of the absorbing gas from the slope of this dependence and after calibration of the PA spectrometer, we can readily find the absorption coefficient of the gas mixture under study for radiation of the given wavelength.

The PA spectrometer was calibrated against the well-known radiation absorption by water vapor at the 694.380-nm H_2O absorption line.

In the case of nonmonochromatic radiation, the amplitude of the PA detector signal U is determined by the convolution integral of the functions describing the shape of the spectral distribution of the absorption coefficient and the spectral distribution of the laser pulse energy[9]:

$$U = \alpha \int_{\Delta\lambda} k(\lambda_0)\, g(\lambda, \lambda_0)\, E(\lambda_l)\, f(\lambda, \lambda_l)\, d\lambda, \qquad (1)$$

where α is the PA spectrometer sensitivity, in V·cm·J^{-1}; $g(\lambda, \lambda_0)$ is the shape of the spectral distribution of the absorption coefficient; $f(\lambda, \lambda_l)$ is the shape of the spectral distribution of the laser pulse energy meeting the normalization condition:

$$\int_{\Delta\lambda} E(\lambda_l)\, f(\lambda, \lambda_l)\, d\lambda = E, \qquad (2)$$

where E is the laser pulse energy; $\Delta\lambda$ is the wavelength range of the laser pulse.

Since at the total pressure of the mixture $P_{tot} \approx 1$ bar the collisional width of the H_2O absorption line is four to five times larger than the Doppler width, the shape of the spectral distribution of the absorption coefficient is close to the Lorentz function (g_L). The ruby laser pulse spectrum, recorded in our experiment by the Fabry–Perot interferometer with the base length t = 30 mm, consists of one component. The energy distribution in the spectrum is described with the high accuracy by the Gauss function (f_G) with the FWHM $\delta\lambda \approx 2.5 \cdot 10^{-3}$ nm. Taking into account the above-said, we can represent Eq. (1) as:

$$\alpha^{-1} = (E/U) \int_{\Delta\lambda} k(\lambda_0)\, g_L(\lambda, \lambda_0)\, f_G(\lambda, \lambda_l)\, d\lambda. \qquad (3)$$

The integral in Eq. (3) is the absorption coefficient distorted by the spectrometer instrumental function $f_G(\lambda, \lambda_l)$. Hereinafter, we refer to this parameter as the effective absorption coefficient and define it as:

$$k_{eff} = U/\alpha E. \qquad (4)$$

Our calculations have shown that as the radiation wavelength varies in the range of variability of the

nonresonant absorption coefficient $\lambda = (694.300 \pm \pm 0.001)$ nm, where its variation does not exceed 1%, k_{eff} coincides, with a high degree of accuracy, with the true value of the absorption coefficient. An example of (U/E) as a function of the relative wavelength shift, recorded with the Fabry–Perot interferometer having the base length $t = 30$ mm, is depicted in Fig. 3.

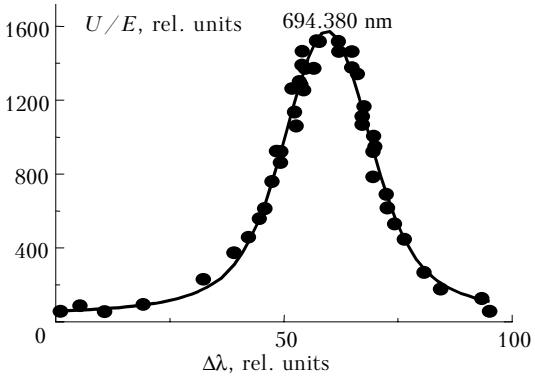

Fig. 3. Profile of the 694.380-nm water vapor absorption line at $P_{\text{tot}} = 270$ mbar and $P_{H_2O} = 14.7$ mbar. The measurements were conducted with the Fabry–Perot interferometer having the base length $t = 30$ nm. Experiment (circles) and Voigt profile (solid line).

Thus, after measurement of $(U^{\max}/E)$ and calculation of the effective absorption coefficient at the line peak for several values of the gas mixture humidity, we can find the PA spectrometer sensitivity with the highest accuracy possible for the given measurement technique. Having measured (U/E) for several values of humidity in the case of nonresonant absorption by Eq. (4) we can readily determine the nonresonant absorption coefficient.

Technique for calculation of absorption coefficient

The molecular absorption coefficients were calculated by the line-by-line method using the software package described in Ref. 19 and HITRAN-96 database.[11] The absorption coefficient was determined as a sum of contributions from lines falling in the wavelength range $\lambda \approx (694 \pm 25)$ nm:

$$k(\lambda) = \sum_{ij} S_{ij}\, f(\lambda_{ij} - \lambda)\, P_j, \qquad (5)$$

where λ_{ij} and S_{ij} are the position and intensity of the ith line of the jth gas; P_j is the partial pressure of the jth gas; $f(\lambda_{ij} - \lambda)$ is the function describing the absorption line shape. The absorption line shape near its peak is described by the Lorentz profile, and some deviations from this profile are usually observed at the 3–5 cm^{-1} tuning away from the resonant frequency. Therefore, in the practical modeling, the absorption coefficient is usually divided into the selective part calculated by Eq. (5) and the continuum part originating from far non-Lorentz wings. In this case, the molecular absorption coefficient is represented as

$$k(\lambda) = k_s(\lambda) + k_c(\lambda), \qquad (6)$$

where k_s and k_c are the selective and continuum absorption coefficients.

For calculation of the continuum absorption coefficient, we used the CKD0 model,[12] which allowed close agreement between the experimentally measured spectra of solar radiation and calculations in the spectral range from 1 to 5 μm (Ref. 20).

The HITRAN-96 database gives the width of the H_2O spectral line centered at $\lambda_0 = 694.380$ nm with the error of 5–10% and the line intensity error higher than 20%.

To minimize the calibration error of the PA spectrometer, we used the intensity and coefficients of collisional broadening of the line centered at $\lambda_0 = 694.380$ nm by the nitrogen and air pressure. These parameters were measured with a spectrophotometer having the resolution of $10^{-3}\,\text{cm}^{-1}$ (Ref. 15). With allowance for the data of Ref. 15, the error of calculation of the effective absorption coefficient at the absorption line peak did not exceed 16%.

The subsequent modeling has shown that the line peak absorption calculated with the data from Ref. 15 is roughly 20% lower than that calculated with data from the HITRAN-96 database.

Results and discussion

Figure 4 depicts the dependence of the measured parameter $(U^{\max}/E)$ at the center of the 694.380-nm H_2O absorption line on the effective absorption coefficient calculated using the data of Ref. 15 at the line peak for mixtures of H_2O with indoor air. Figures 5 and 6 depict the coefficients of nonresonant absorption of the 694.300 nm radiation by the binary mixtures of H_2O with indoor air and nitrogen as functions of the water vapor partial pressure, as well as the calculated coefficients of nonresonant absorption allowing for and neglecting the water vapor continuum absorption.

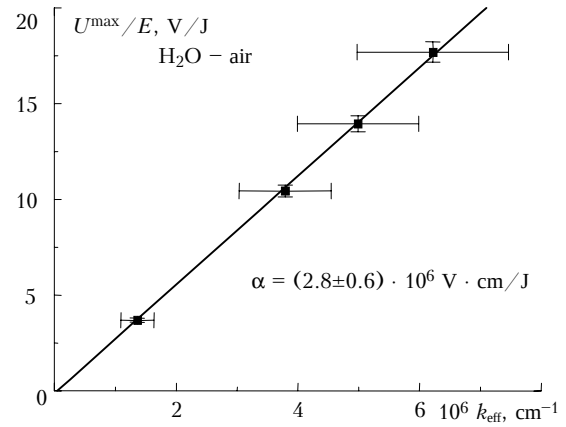

Fig. 4. The PA spectrometer signal $(U^{\max}/E)$ vs. the effective absorption coefficient. The signal $(U^{\max}/E)$ was measured and k_{eff} was calculated for 694.380-nm H_2O absorption line peak at the total pressure of the mixture of water vapor and indoor air $P_{\text{tot}} = 1005$ mbar and the temperature $T = 298$ K.

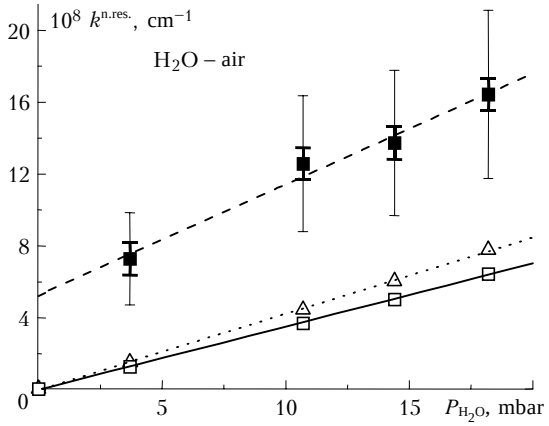

Fig. 5. Coefficient of radiation absorption at the wavelength of 694.300 nm by atmospheric air at the pressure P_{tot} = 1005 mbar and the temperature T = 298 K vs. the air humidity: experiment (■), calculation with allowance for H_2O continuum absorption (Δ), calculation neglecting H_2O continuum absorption (□).

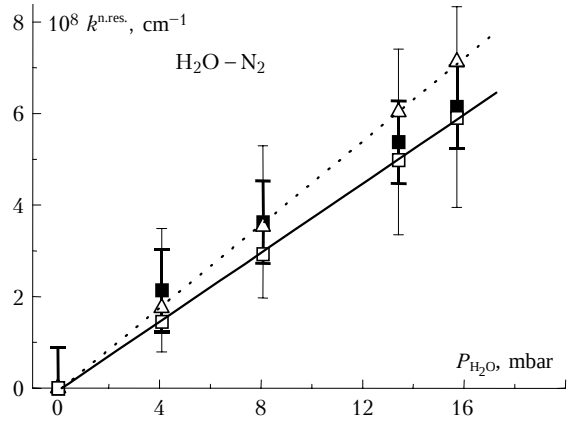

Fig. 6. Coefficient of radiation absorption at the wavelength 694.300 nm by the H_2O–nitrogen mixture at the pressure P_{tot} = 945 mbar and the temperature T = 298 K vs. the H_2O partial pressure: experiment (■), calculation with allowance for H_2O continuum absorption (Δ), calculation neglecting H_2O continuum absorption (□).

The plots were obtained in the following way. The ruby laser was tuned in resonance with the 694.380-nm H_2O absorption line with corresponding attaining of the PA signal maximum amplitude U^{max} recorded by the S9-16 oscilloscope. The typical signal is presented in Fig. 7 (curve *1*). Then the PA detector cell was pumped down and several times "washed" by nitrogen until the PA signal amplitude U^{max} became zero. Finally, the cell was evacuated down to the pressure $P_{tot} \le 0.03$ mbar. Thereafter it was sequentially filled with indoor air and water vapor from a cylinder with distilled water in the liquid phase. The final pressure of the gas mixture in the cell was equal to the atmospheric pressure.

Varying the ruby laser radiation wavelength from pulse to pulse, we recorded the spectral distribution of (U/E) (see Fig. 3) and determined (U^{max}/E). Then the laser was tuned to the wavelength λ = 694.300 nm, and we measured (U/E) for the case of nonresonant absorption. The PA signal shape for nonresonant absorption of radiation by the air–water vapor mixture is shown as curve *2* in Fig. 7. Since the amplitude of the valid PA signal in the case of nonresonant absorption only several times exceeded the noise level, we accumulated 25 PA signals in the memory of the S9-16 digital oscilloscope (see Fig. 7, curves *3–5*) to five-fold increase the signal-to-noise ratio. Such a procedure of measuring the PA signals of the resonant and nonresonant absorption was repeated at several values of the indoor air humidity.

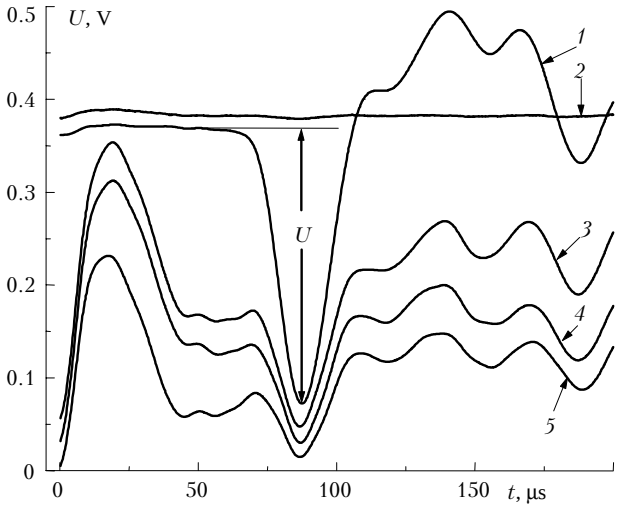

Fig. 7. Time scanning of the PA detector signal: signal for the radiation resonant with the 694.380-nm H_2O absorption line (curve *1*) and signals for nonresonant radiation with the wavelength of 694.300 nm (curves *2–5*), PA detector response to one pulse (*1*, *2*) and sum of 25 PA signals (*3–5*).

Using the measured signals of the resonant absorption, we plotted the dependence of (U^{max}/E) on the effective absorption coefficient (see Fig. 4). This dependence was used to determine the spectrometer sensitivity α. (In the experiments with water vapor and indoor air, the sensitivity was $\alpha = (2.8 \pm 0.6)\cdot 10^6$ V·cm/J.) Then the value of α was used to determine the coefficient of nonresonant radiation absorption at the wavelength of 694.300 nm by indoor air and its dependence on the water vapor partial pressure (see Fig. 5).

Similar measurements were conducted for the mixture of H_2O with nitrogen.

The measurement error of the nonresonant absorption coefficient includes the calibration error of the PA spectrometer and the measurement error of (U/E) in relative units for the 694.300 nm radiation. The calibration error, in its turn, includes the error of calculation of the effective absorption coefficient at H_2O 694.380-nm absorption line peak and the measurement errors of (U^{max}/E). The error of calculation of the effective absorption coefficient at the line peak for the H_2O–nitrogen mixture, used in the experiment, consists of the error of the initial spectroscopic data (≤ 16%) (Ref. 15) and the error of measuring the H_2O concentration in mixtures. The water vapor concentration in mixtures was measured

using an oil gauge with the error not exceeding 2%. For the experiments with air, this error should be complemented with the error of the air humidity measurement with the Assman aspiration psychrometer, which makes up 2%. In Fig. 4, the error of calculation of the effective absorption coefficient is shown by the horizontal confidence intervals.

Since the PA signal amplitudes $U^{\max}$ and E exceeded the noise level by two to three orders of magnitude, the error of relative measurements ($U^{\max}/E$), was determined only by specifications of the oscilloscopes S9-16 and S9-8 and did not exceed 3%. In Fig. 4, this error is shown by the vertical confidence intervals. Thus, the resulting calibration error of the PA spectrometer does not exceed 21% for the mixtures of H_2O with nitrogen and 23% for the mixtures of H_2O with air.

In U/E measurements corresponding to the weak nonresonant absorption, the main source of error is the noise level of the PA detector. In the experiment, the signal with the amplitude $U = 4 - 5$ mV was distinguished against the noise background. Thus, to estimate the error, we can consider the noise magnitude equal to ± 2.5 mV. Based on this level of noise, the measurement errors for nonresonant absorption coefficients were calculated in relative units with allowance for accumulation of 25 pulses. These errors are independent of the water vapor concentration (the absorption signal amplitude). In Figs. 5 and 6 they are shown as bold vertical intervals. The total measurement errors for nonresonant absorption coefficients are depicted in Figs. 5 and 6 as vertical confidence intervals. It is seen that at zero error in the spectrometer calibration constant, the minimal absorption coefficient obtained in this work is $k_\lambda^{\min} \le 10^{-8}$ cm^{-1}.

For illustration, all signals depicted in Fig. 7 are spaced apart along the ordinate. It is seen that in the case of nonresonant absorption (curves *3–5*) the shape of PA signals is very close to the PA signal's shape of the resonant absorption (curve *1*), starting from the time $t = 50$ μs. This indicates that the signals are of the same origin, namely, absorption of radiation by the gas mixture under study. At the same time, at $t < 50$ μs the signal of positive polarity (curves *3–5*) is clearly seen in the time scanning of the PA signals of the nonresonant absorption. This signal is feeble against the background of the high-amplitude negative PA resonant absorption signal (curve *1*) of negative polarity.

In this paper, we do not dwell on the causes and mechanism of generation of this signal. We only note that it was found experimentally that the signal of positive polarity is connected with the radiation scattering by both the cell windows and the gas under study.

The modeling have shown that the contribution of continuum to the total absorption in the considered spectral range is relatively small. For the 694.300 nm radiation, it is roughly 20% and lies within the limits of the experimental error (see Figs. 5 and 6), and it is negligibly small for the absorption line centered at 694.380 nm and used for calibration of the PA spectrometer (see Fig. 2*a*).

Figure 6 shows that the nonresonant radiation absorption coefficients (694.300 nm) for the binary H_2O–nitrogen mixtures coincide, within the measurement errors, with the absorption coefficients calculated allowing for and neglecting the water vapor continuum absorption. Therefore, the true value of the continuum absorption in this spectral range and its role in the shortwave radiation extinction by the atmosphere is still an open question. To answer it, the spectrometer sensitivity should be increased by an order of magnitude and the total error in the spectroscopic data used for calibration of the spectrometer should be decreased down to ≤ 5%.

At the same time, Fig. 5 shows that the experimental absorption coefficient obtained for the mixtures of water vapor with indoor air exceeds the absorption coefficient calculated both allowing for and neglecting the water vapor continuum absorption. The difference between the experimental values and those calculated with allowance for the H_2O continuum increases from $5.8 \cdot 10^{-8}$ cm^{-1} to $8.6 \cdot 10^{-8}$ cm^{-1} as the air humidity increases from $P_{H_2O} = 3.8$ mbar to $P_{H_2O} = 18.2$ mbar and exceeds the absolute measurement error.

The results obtained in this work well agree with the results of Ref. 1 and confirm the conclusion on the presence of some atmospheric constituent responsible for the excess atmospheric absorption of shortwave radiation, different from the molecular absorption.[1]

In Ref. 1 it was shown that the excess absorption of shortwave radiation in the atmosphere is most probably caused by the fine soot aerosol. Therefore, in our further research we plan to measure the coefficient of nonresonant absorption of visible radiation by atmospheric air as a function of the concentration of the fine soot aerosol in it.

Conclusion

Modernization of the PA spectrometer with a monopulse ruby laser and improvement of the measurement technique allowed us to reach the threshold sensitivity of $k_\lambda^{\min} \le 10^{-8}$ cm^{-1} for the absorption coefficient. Using the PA spectrometer, we have measured the coefficient of weak nonresonant radiation absorption at the wavelength $\lambda = 694.300$ nm by the binary mixtures of water vapor with nitrogen and atmospheric (indoor) air as a function of the water vapor concentration. The measurements were conducted at the total gas pressure in the PA cell $P_{tot} \approx 1$ bar.

The results obtained confirm the conclusion[1] that the excess atmospheric absorption of shortwave radiation is caused by some atmospheric substance responsible for non-molecular absorption.

Acknowledgments

The authors are thankful to Yu.A. Pkhalagov for useful consultations and fruitful discussions.

This work was partly supported by the Russian Foundation for Basic Research (Grant No. 99–05–64564).

References

1. Yu.A. Pkhalagov, V.N. Uzhegov, and N.N. Shchelkanov, Atmos. Oceanic Opt. **11**, No. 4, 272–276 (1998).
2. H. Chen and D. Lu, in: *Proc. of the International Radiation Symposium IRS – 96: Current Problems in Atmospheric Radiation* (Fairbanks, Alaska, 1996), pp. 1042–1045.
3. K.Ya. Kondratjev, V.I. Binenko, and I.N. Melnikova, Meteorol. Gidrol., No. 2, 14–23 (1996).
4. C. Tomasi, R. Guzzi, and O. Vittori, J. Atmos. Sci. **31**, 255–260 (1974).
5. Yu.A. Pkhalagov, V.N. Uzhegov, and N.N. Shchelkanov, Atmos. Oceanic Opt. **7**, No. 10, 714–720 (1994).
6. Yu.A. Pkhalagov, V.N. Uzhegov, and N.N. Shchelkanov, Atmos. Oceanic Opt. **9**, No. 6, 455–458 (1996).
7. L.I. Nesmelova, O.B. Rodimova, and S.D. Tvorogov, Atmos. Oceanic Opt. **10**, No. 2, 81–83 (1997).
8. L.I. Nesmelova, Yu.A. Pkhalagov, O.B. Rodimova, S.D. Tvorogov, V.N. Uzhegov, and N.N. Shchelkanov, Atmos. Oceanic Opt. **12**, No. 3, 278–284 (1999).
9. B.G. Ageev, Yu.N. Ponomarev, and B.A. Tikhomirov, *Nonlinear Photo-Acoustic Spectroscopy of Molecular Gases* (Nauka, Novosibirsk, 1987), 128 pp.
10. V.A. Pilipovich and A.A. Kovalev, *Optical Lasers with Antireflection Filters* (Nauka i Tekhnika, Minsk, 1975), 216 pp.
11. L.S. Rothman, C.P. Rinsland, A. Goldman, S.T. Massie, D.P. Edwards, J.-M. Flaud, A. Perrin, C. Camy-Peyret, V. Dana, J.-Y. Mandin, J. Schroeder, M. McCann, R.R. Gamache, R.B. Wattson, K. Yoshino, K.V. Chance, K.W. Jucks, L.R. Brown, V. Nemtchinov, and P. Varanasi, J. Quant. Spectrosc. Radiat. Transfer **60**, No. 6, 665–710 (1998).
12. S. Clough, F. Kneizis, and R. Davies, Atmos. Res., No. 23, 229–241 (1989).
13. R.K. Long, *Atmospheric Absorption of Laser Radiation*, Engineering Publication Bull. No. 199 (Ohio State Univ., Ohio, 1966), 24 pp.
14. M.M. Johnson and A.H. La Grone, Radio Sci. **8**, No. 5, 407–410 (1973).
15. I.S. Tyryshkin, *"Study of line broadening of atmospheric water vapor in the visible region by the method of high-resolution laser spectroscopy,"* Author's Abstract of Cand. Phys. Math. Sci. Dissert., Tomsk (1983), 19 pp.
16. B.A. Tikhomirov, Yu.N. Ponomarev, and V.A. Dolgikh, Zh. Prikl. Spektrosk. **34**, No. 4, 653–656.
17. S.L. Bragg, S.A. Lawton, and C.E. Wiswall, Opt. Lett. **10**, No. 7, 321 (1985).
18. E.A. Korotchenko, A.Yu. Kurov, V.D. Nikolaev, Yu.N. Ponomarev, M.I. Svistun, and B.A. Tikhomirov, Opt. Atm. **1**, No. 1, 139–141 (1988).
19. A.A. Mitsel', I.V. Ptashnik, K.M. Firsov, and B.A. Fomin, Atmos. Oceanic Opt. **8**, No. 10, 847–848 (1995).
20. P.D. Brown, S.A. Clough, E.J. Mlawer, T.R. Ghipper, and F.J. Murcray, in: *Proc. of the Eighth Atmospheric Radiation Measurement (ARM) Science Team Meeting* (Tuscon, Arisona, 1998), pp. 101–108.